An interactive GUI to control an SLM for STED microscopy and adaptive optics

Wiebke Jahr
wiebke.jahr@web.de
https://github.com/wiebkejahr/slm_control

June 6, 2022

1 Rationale

For several centuries, diffraction of light was believed to fundamentally limit the resolution of light microscopy – a limit which has since been shattered by various super-resolution microscopies [1]. In theory, the attainable resolution is infinite; yet high light intensities and optical aberrations hinder the separation of fine features [2, 3, 4].

In STED microscopy, a light pattern drives fluorescent molecules from the signalling excited state to the dark ground state, except for the tightly confined volume around intensity minima [5, 6]. The most widely used light patterns are created using a vortex-phasemask, resulting in a "doughnut"-shaped focus to constrict the fluorescent volume in the image plane (called xy-STED here) or a top-hat phasemask for strong resolution increase along the optical axis and moderate increase within the image plane (z-STED) [7]. Both patterns are exquisitely sensitive to aberrations, as has been studied in great detail through simulations [8, 9, 10, 11, 12]. Specifically, aberrations "filling" the zero intensities of the STED patterns result in a decrease of signal, increase of state cycling and phototoxicity [13].

Many aberrations can be identified and corrected for through meticulous alignment of the microscope system before the start of an experiment. Since the image formation is strongly dominated by the STED beams [14], it is sufficient to correct aberrations in these [15]. Many modern STED microscopes are equipped with a spatial light modulator (SLM) displaying phasemasks to create the STED intensity patterns [16], where it is straightforward to add aberration correction to the vortex or top-hat patterns [17] and to adjust the overlay of the excitation and depletion beams [18].

To ease manual alignment, the relevant parameters governing the STED intensity patterns need to be accessible via an intuitive and responsive user interface. I designed an SLM control software centred around an interactive GUI. The holographic phase patterns are calculated in a computation-time efficient way, and the SLM display is updated on the fly, thus making manual alignment of the STED beam convenient.

2 Required Packages and Installation

The software is written in python (3.9.0) [19] using numpy (1.22.1) [20, 21, 22] for pattern calculations. The GUI is designed using pyqt5 (5.15.6) [23]. Matplotlib 3.5.1 [24] and Pillow 9.0.0 [25] are used for image display. The code was tested both on homebuilt STED microscopes, running the SLM as an external display, and on an Abberior Expert Line STED microscope, using Abberior's API (specpy, version 1.2.1) to control the SLM. Specpy requires older versions of numpy (1.16.xx), so the installation was modified accordingly.

3 Optical setup

The control suite can be run stand-alone for homebuilt systems where patterns are displayed full screen via the graphics output with the SLM controller attached, but is just as easily integrated into any existing microscopy control suite featuring an API, if e. g. a commercial microscope is to be upgraded with an SLM. The code supports permanent storage of default parameters (in .json format, via export of python dictionaries) and supports the usage of multiple objectives, each one with its own parameters.

The SLM can be run in a single image geometry, where the laser beam is reflected once off the SLM. Alternatively, the SLM area can be used to display a "split" image, where each half displays a different phase pattern, for example to overlay xy and z STED patterns using only a single SLM. The optical layout could use two STED lasers (or the same laser split into two fibers), modulate their phase with the SLM and combine with a polarizing beamsplitter cube afterwards. Alternatively, the SLM can run in a double pass geometry, where the laser is reflected twice off the SLM. Polarisation is rotated 90° in-between passes, such that the two phase patterns are imprinted on orthogonal polarisations achieving incoherent superposition of the light distributions [17]. The relative contributions between the two patterns are tuned by rotating a half-wave plate to adjust polarisation direction, but total STED power remains constant.

4 Pattern creation

The incident laser beam tends to drift continuously, e. g. due to temperature fluctuations. Therefore, the position of the phasemask with respect to the incident beam requires frequent realignment. Thus, a responsive GUI and fast recalculation is especially important. To avoid computationally expensive re-calculation of the whole pattern as well as discontinuities at the edge of the patterns, all phasemasks are created at double the size required, and cropped to their actual size with a variable center position whenever the offset is changed. With this design, the center position phasemask is quickly adjusted.

The SLM can be run in single or split image geometry. Change of SLM layout requires a restart of the code, and changing the boolean "split image" parameter in the `parameters_general.txt` file before restarting. The "Flatfield" checkbox activates ad-

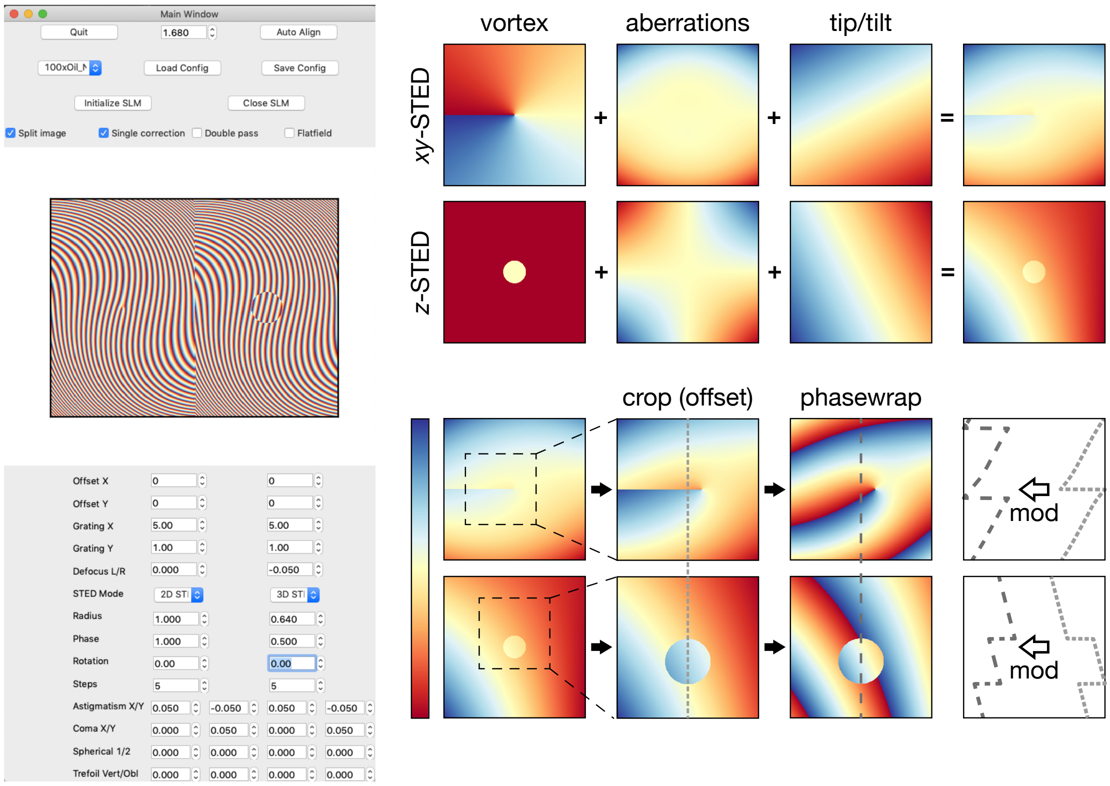

Figure 1: SLM control code. *Left:* GUI main window. *Top*: General controls to start/stop communication with SLM, select the objective and load/store configurations. *Center:* Preview of the SLM display. *Bottom:* Controls to describe the pattern.
Right:

dition of the flatfield correction image (see below). For a double-pass geometry, where the same laser beam bounces twice off the SLM, identical aberration correction is often needed for both passes. Activating the "single correction" checkbox provides a convenient means to do so. Likewise, activating the "double pass" checkbox duplicates and re-applies the flatfield correction (see below).

Each of these SLM half-patterns is composed of several sub-patterns (Figure 1B):

First, the phase mask to create the different STED distributions. If left blank, a standard Gaussian focus was formed; vortex and top-hat pattern created the xy-and z-STED patterns. Further, I implemented segmented (easy STED, [26]) and bivortex phasemasks (coherent hybrid STED, [27]). Full flexibility is provided by the options to enter python source code describing a pattern or uploading an image displaying the phase mask.

Second, aberration corrections are described via a weighted sum of Zernike polynomials. While other parametrisations exist, Zernike polynomials are most widespread in the adaptive optics community because they are orthonormal, intuitive in their taxonomy and approximate the aberrations commonly encountered in microscopy with a finite subset [3].

$$Z = \sum_{[0,0]}^{[m,n]} a_n^{\pm m} \cdot Z_n^{\pm m}\left(\rho, \varphi\right) \tag{1}$$

with

$$\begin{aligned} Z_n^m\left(\rho, \varphi\right) = &\quad R_n^m\left(\rho\right) \cos\left(m\varphi\right) \\ Z_n^{-m}\left(\rho, \varphi\right) = &\quad R_n^m\left(\rho\right) \sin\left(m\varphi\right) \end{aligned} \tag{2}$$

and

$$R_n^m\left(\rho\right) = \sum_{k=0}^{\frac{n-m}{2}} \frac{\left(-1\right)^k\left(n-k\right)!}{k!\left(\frac{n+m}{2}-k\right)!\left(\frac{n-m}{2}-k\right)!} \rho^{n-2k} \tag{3}$$

The weights of the most common aberrations (astigmatism, coma, spherical and trefoil) are accessible via the GUI. All others are implemented via their radial and azimuthal indices and are easily accessible via the source code window if needed.

Third, all patterns are created holographically to separate the first order from the undiffracted/unmodulated beam by adding a blazed grating [28]. Conveniently, this corresponds to tip and tilt of a mirror, implemented here as Zernike polynomials Z_1^{-1} and Z_1^1. The holographic layout is further useful to align the position of the first diffraction order (i. e. the STED beam focus) perfectly with the excitation beams [18], simply by changing the pitch of the grating slightly.

Fourth, a flatfield correction image can be loaded to correct for imperfections of the SLM surface (not shown in figure). If the SLM is operated in a double pass geometry, the flatfield correction is only imprinted on the polarization currently aligned with the SLM. Therefore, an option is implemented to split the flatfield correction pattern and apply it again on the second half with the appropriate offset.

In order to minimize computational time, and to keep the GUI responsive, I am storing all four subpatterns separately in the control PC's memory. Whenever any of the parameters are changed the GUI, only the relevant subpatterns are updated and all subpatterns are added to compute the complete phasemask. Finally, the patterns are cropped to half their size to account for the offset, phasewrapped to unit brightness and scaled to match the SLM stroke to the wavelength of the STED beam.

5 Permanent parameter storage

6 APGL Licence

Funding W.J. gratefully acknowledges funding by a Human Frontier Science Program long term fellowship (HFSP LT000557/2018).

Data Availability Statement All code is available under the following link: `https://github.com/wiebkejahr`

References

[1] S.W. Hell, S.J. Sahl, M. Bates, X. Zhuang, R. Heintzmann, M.J. Booth, J. Bewersdorf, G. Shtengel, H. Hess, P. Tinnefeld, A. Honigmann, S. Jakobs, I. Testa, L. Cognet, B. Lounis, H. Ewers, S.J. Davis, C. Eggeling, D. Klenerman, K.I. Willig, G. Vicidomini, M. Castello, A. Diaspro, *&* T. Cordes The 2015 super-resolution microscopy roadmap. *Journal of Physics D: Applied Physics* **48**(44) (2015), 443001. DOI: `10.1088/0022-3727/48/44/443001`.

[2] M.J. Booth Adaptive optics in microscopy. *Philosophical Transactions of the Royal Society A: Mathematical, Physical and Engineering Sciences* **365**(1861) (Sept. 2007), 2829–2843. DOI: `10.1098/rsta.2007.0013`.

[3] J.A. Kubby *Adaptive optics for biological imaging.* CRC press, 2013.

[4] M.J. Booth Adaptive optical microscopy: the ongoing quest for a perfect image. *Light: Science & Applications* **3**(4) (2014), e165. DOI: `10.1038/lsa.2014.46`.

[5] S.W. Hell *&* J. Wichmann Breaking the diffraction resolution limit by stimulated emission: stimulated-emission-depletion fluorescence microscopy. *Optics Letters* **19**(11) (1994), 780–782. DOI: `10.1364/ol.19.000780`.

[6] T.A. Klar, S. Jakobs, M. Dyba, A. Egner, *&* S.W. Hell Fluorescence microscopy with diffraction resolution barrier broken by stimulated emission. *Proc. Natl. Acad. Sci.* **97**(15) (2000), 8206–8210. DOI: `10.1073/pnas.97.15.8206`.

[7] J. Keller, A. Schönle, *&* S.W. Hell Efficient fluorescence inhibition patterns for RESOLFT microscopy. *Optics Express* **15**(6) (2007), 3361. DOI: `10.1364/oe.15.003361`.

[8] S. Deng, L. Liu, Y. Cheng, R. Li, *&* Z. Xu Effects of primary aberrations on the fluorescence depletion patterns of STED microscopy. *Optics Express* **18**(2) (2010), 1657–1666. DOI: `10.1364/oe.18.001657`.

[9] B.R. Patton, D. Burke, R. Vrees, & M.J. Booth Is phase-mask alignment aberrating your STED microscope? *Methods and Applications in Fluorescence* **3**(2) (2015), 024002. DOI: `10.1088/2050-6120/3/2/024002`.

[10] J. Antonello, E.B. Kromann, D. Burke, J. Bewersdorf, & M.J. Booth Coma aberrations in combined two- and three-dimensional STED nanoscopy. *Optics Letters* **41**(15) (2016), 3631. DOI: `10.1364/ol.41.003631`.

[11] J. Antonello, D. Burke, & M.J. Booth Aberrations in stimulated emission depletion (STED) microscopy. *Optics Communications* **404** (2017), 203–209. DOI: `10.1016/j.optcom.2017.06.037`.

[12] Y. Li, H. Zhou, X. Liu, Y. Li, & L. Wang Effects of aberrations on effective point spread function in STED microscopy. *Applied Optics* **57**(15) (2018), 4164. DOI: `10.1364/ao.57.004164`.

[13] W. Jahr, P. Velicky, & J.G. Danzl Strategies to maximize performance in STimulated Emission Depletion (STED) nanoscopy of biological specimens. *Methods* (July 2019). DOI: `10.1016/j.ymeth.2019.07.019`.

[14] B. Harke, J. Keller, C.K. Ullal, V. Westphal, A. Schönle, & S.W. Hell Resolution scaling in STED microscopy. *Optics Express* **16**(6) (2008), 4154–4162. DOI: `10.1364/oe.16.004154`.

[15] M. Booth, D. Andrade, D. Burke, B. Patton, & M. Zurauskas Aberrations and adaptive optics in super-resolution microscopy. *Microscopy* **64**(4) (June 2015), 251–261. DOI: `10.1093/jmicro/dfv033`.

[16] E. Auksorius, B.R. Boruah, C. Dunsby, P.M.P. Lanigan, G. Kennedy, M.A.A. Neil, & P.M.W. French Stimulated emission depletion microscopy with a supercontinuum source and fluorescence lifetime imaging. *Optics Letters* **33**(2) (2008), 113. DOI: `10.1364/ol.33.000113`.

[17] M.O. Lenz, H.G. Sinclair, A. Savell, J.H. Clegg, A.C.N. Brown, D.M. Davis, C. Dunsby, M.A.A. Neil, & P.M.W. French 3-D stimulated emission depletion microscopy with programmable aberration correction. *Journal of Biophotonics* **7**(1-2) (2013), 29–36. DOI: `10.1002/jbio.201300041`.

[18] T.J. Gould, E.B. Kromann, D. Burke, M.J. Booth, & J. Bewersdorf Auto-aligning stimulated emission depletion microscope using adaptive optics. *Optics Letters* **38**(11) (2013), 1860–1862. DOI: `10.1364/ol.38.001860`.

[19] Python *Python Language Reference, version 2.7.* Python Software Foundation. 2013. `http://www.python.org`. Accessed on 2016-09-18.

[20] Numpy *is the fundamental package for scientific computing with Python.* 2016. `http://www.numpy.org/`. Accessed on 2016-11-21.

[21] S. van der Walt, S.C. Colbert, & G. Varoquaux The NumPy Array: A Structure for Efficient Numerical Computation. *Computing in Science & Engineering* **13**(2) (Mar. 2011), 22–30. DOI: `10.1109/mcse.2011.37`.

[22] C.R. Harris, K.J. Millman, S.J. van der Walt, R. Gommers, P. Virtanen, D. Cournapeau, E. Wieser, J. Taylor, S. Berg, N.J. Smith, R. Kern, M. Picus, S. Hoyer, M.H. van Kerkwijk, M. Brett, A. Haldane, J.F. del Río, M. Wiebe, P. Peterson, P. Gérard-Marchant, K. Sheppard, T. Reddy, W. Weckesser, H. Abbasi, C. Gohlke, *&* T.E. Oliphant Array programming with NumPy. *Nature* **585**(7825) (Sept. 2020), 357–362. DOI: `10.1038/s41586-020-2649-2`.

[23] R.C. Limited *PyQt5*. `https://www.riverbankcomputing.com/software/pyqt/` ..

[24] J.D. Hunter Matplotlib: A 2D Graphics Environment. *Computing in Science & Engineering* **9**(3) (2007), 90–95. DOI: `10.1109/mcse.2007.55`.

[25] A. Clark *Pillow (PIL Fork) Documentation*. 2015. `https://buildmedia.readthedocs.org/media/pdf/pillow/latest/pillow.pdf`.

[26] F. Görlitz, P. Hoyer, H. Falk, L. Kastrup, J. Engelhardt, *&* S.W. Hell A STED microscope designed for routine biomedical applications. *Progress In Electromagnetics Research* **147** (2014), 57–68. DOI: `10.2528/pier14042708`.

[27] A. Pereira, M. Sousa, A.C. Almeida, L.T. Ferreira, A.R. Costa, M. Novais-Cruz, C. Ferrás, M.M. Sousa, P. Sampaio, M. Belsley, *&* H. Maiato Coherent-hybrid STED: high contrast sub-diffraction imaging using a bi-vortex depletion beam. *Optics Express* **27**(6) (2019), 8092. DOI: `10.1364/oe.27.008092`.

[28] Neil, Wilson, *&* Juskaitis A wavefront generator for complex pupil function synthesis and point spread function engineering. *Journal of Microscopy* **197**(3) (Mar. 2000), 219–223. DOI: `10.1046/j.1365-2818.2000.00680.x`.